Adhesive joint design methods and examples

Pavlovic, M.; Christoforidou, A.; Keller, Thomas

Publication date
2022

Document Version
Final published version

Published in
Proceedings of the 20th European Conference on Composite Materials: Composites Meet Sustainability

Citation (APA)
Pavlovic, M., Christoforidou, A., & Keller, T. (2022). Adhesive joint design methods and examples. In A. P. Vassilopoulos , & V. Michaud (Eds.), *Proceedings of the 20th European Conference on Composite Materials: Composites Meet Sustainability: Vol 5 – Applications and Structures* (pp. 615-622). EPFL Lausanne, Composite Construction Laboratory.

ECCM

20

26-30 JUNE

2022

LAUSANNE

SWITZERLAND

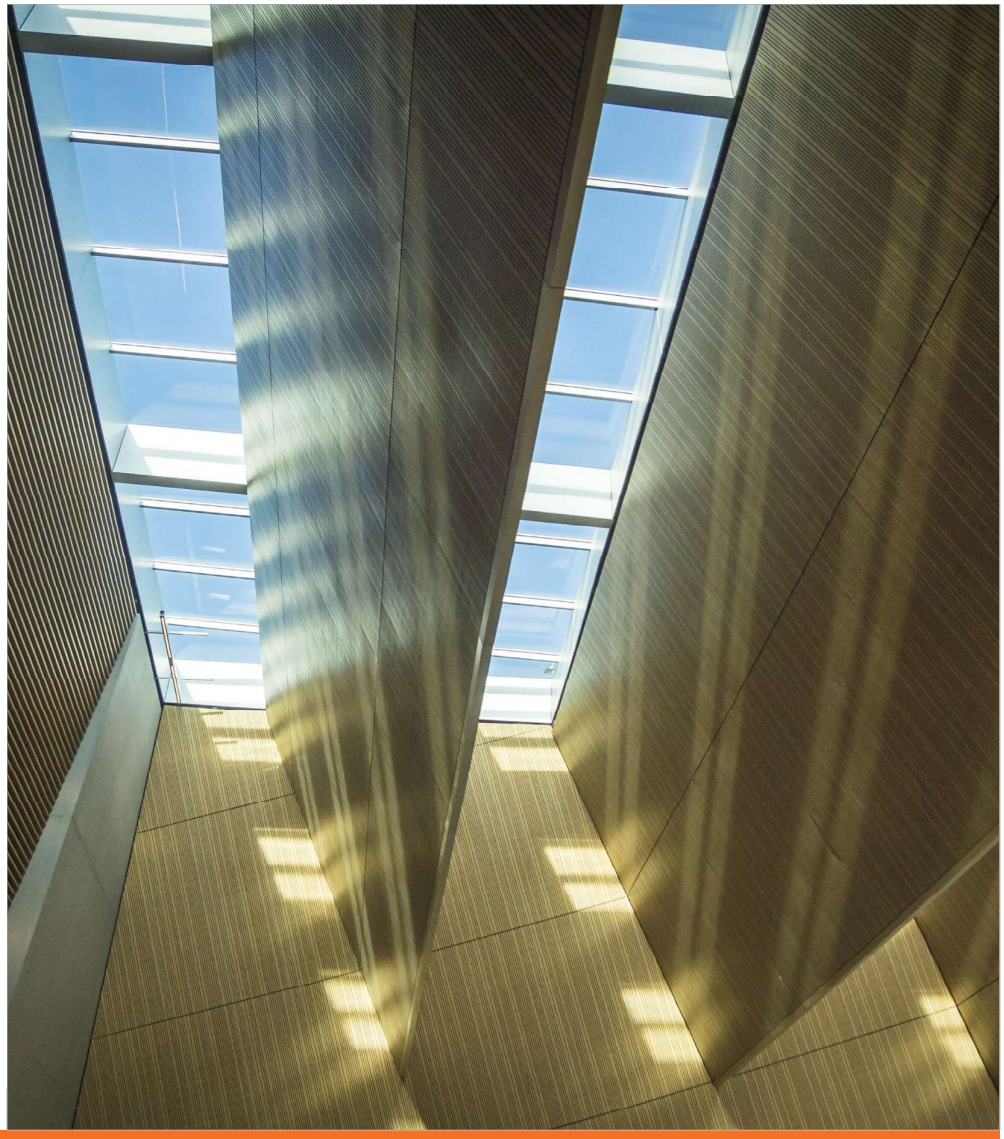

Proceedings of the 20th European Conference on Composite Materials

COMPOSITES MEET SUSTAINABILITY

Vol 5 – Applications and Structures

Editors : Anastasios P. Vassilopoulos, Véronique Michaud

Organized by :

EPFL

Under the patronage of :

CCLAB Composite Construction Laboratory

LPAC Laboratory for Processing of Advanced Composites

ESCM EUROPEAN SOCIETY FOR COMPOSITE MATERIALS

ECCM 20
26-30 JUNE 2022
LAUSANNE SWITZERLAND

EPFL CCLAB Composite Construction Laboratory LPAC Laboratory for Processing of Advanced Composites

Proceedings of the 20th European Conference on Composite Materials ECCM20 26-30 June 2022, EPFL Lausanne Switzerland

Edited By :

Prof. Anastasios P. Vassilopoulos, CCLab/EPFL
Prof. Véronique Michaud, LPAC/EPFL

Oragnized by:

Composite Construction Laboratory (CCLab)
Laboratory for Processing of Advanced Composites (LPAC)
Ecole Polytechnique Fédérale de Lausanne (EPFL)

ISBN: 978-2-9701614-0-0
DOI: http://dx.doi.org/10.5075/epfl-298799_978-2-9701614-0-0

Published by :

Composite Construction Laboratory (CCLab)
Ecole Polytechnique Fédérale de Lausanne (EPFL)
BP 2225 (Bâtiment BP), Station 16
1015, Lausanne, Switzerland

https://cclab.epfl.ch

Laboratory for Processing of Advanced Composites (LPAC)
Ecole Polytechnique Fédérale de Lausanne (EPFL)
MXG 139 (Bâtiment MXG), Station 12
1015, Lausanne, Switzerland

https://lpac.epfl.ch

Cover:

Swiss Tech Convention Center
© Edouard Venceslau - CompuWeb SA

Cover Design:

Composite Construction Laboratory (CCLab)
Ecole Polytechnique Fédérale de Lausanne (EPFL)
Lausanne, Switzerland

©2022 ECCM20/The publishers

Disclaimer:

ADHESIVE JOINT DESIGN METHODS AND EXAMPLES

Marko, Pavlovic[a], Angeliki, Christoforidou[b], Thomas, Keller[c]

a, b: Faculty of Civil Engineering and Geosciences, Delft University of Technology, 2628 CN Delft, Netherlands – M.Pavlovic@tudelft.nl
c: EPFL, Switzerland

Abstract: *Challenges of reliable prediction of resistance of bonded joints lie in the complexity of stress concentrations, multiple crack paths, mode-mixity and sudden crack propagation. The new Technical Specification for Design of fibre-polymer composite structures (TS) is bridging this gap by providing comprehensive sets of design recommendations and analyses to be used for the verification of adhesive joints. Two design approaches in the TS, based on stress analysis and fracture mechanics, are summarized and basic design assumptions on allowed failure conditions and partial factors in relation to execution and maintenance are highlighted.*

The application of the design recommendations is shown on the example of determining the design value and the ultimate resistance of a simple double lap joint. FE models built in Abaqus are used to analyse stress concentrations and crack initiation and propagation based on material level experiments. Variability of the material properties are taken into account through partial safety factors. Joint resistances obtained by the stress-based approach and fracture-mechanics approach are compared.

Keywords: adhesive joints; design recommendation; admissible failure modes; stress analysis; fracture mechanics

1. Introduction

Adhesive bonding in fibre-polymer composite structures can be a competitive connection solution over bolting because of slip resistance, no weakening of the cross section of the laminated composite plate, applicability to curved, tapered or non-plated members, etc. More common application of adhesive bonding in load carrying structural details is hinged by the lack of confidence and established design rules to predict resistance of the joints. The new Technical Specification for Design of fibre-polymer composite structures (TS) is bridging this gap by providing comprehensive sets of design recommendations, requirements and framework of analyses and tests on the joint and material level to be used for the verification of adhesive joints.

2. Design of adhesively bonded joints according to Technical Specification

2.1 Design assumptions

The basic principle is that an adhesive joint shall be designed as fail-safe. A joint failure shall not result in failure (progressive collapse) of the whole structure comprising the joint. Failure of an adhesive joint shall be considered as an accidental situation in accordance with EN 1990. For example, the fail-safe condition can be achieved either by providing an alternative (back-up) load carrying mechanism in the joint, e.g. by making hybrid adhesive-bolted joints and/or by providing redundant degrees of freedom in the structure, e.g. by crossed braces in a truss structure.

  doi:10.5075/epfl-298799_978-2-9701614-0-0

The TS defines permissible failure modes of an adhesive connection being either cohesive failure in the adhesive or fibre-tear failure in the adherend. Pure adhesive failure, i.e. complete failure in the adherend-adhesive interface, shall be avoided through appropriate material selection and surface preparation. Validation of the failure mode by tests is required. It is important to consider that the environmental conditions can change the failure mode.

In general, adhesive joints being symmetrical with regard to the load axis are recommended. Eccentricities in the load transfer should be minimized. A minimum thickness of the adhesive layer of 1.0 mm should be specified and properly verified in the production. Measures of tapering the adherents and/or adhesive fillets can be applied to reduce the stress peaks, however care must be taken that the size effects on strength can limit the effectiveness of such improvements.

2.2 Partial safety factors and conversion factors for adhesive connections

A design value of the adhesive connection resistance $R_{ac,Rd} = R_{ac,k} \cdot \eta_c / \gamma_{M,ac}$ is calculated on the basis of the characteristic value of the adhesive connection resistance $R_{ac,k}$ and partial factor $\gamma_{M,ac}$ and conversion factor η_c. The conversion factor η_c is covering aspects of moisture, temperature and ageing on the matrix-dominated property that causes failure, e.g. for fibre-tear or cohesive failure in the adhesive. A single partial factor $\gamma_{M,ac}$ ranging from 1,5 to 2,5 is used to account for uncertainties related to material, resistance model and factors related to inspection, maintenance, accessibility and control in application. The characteristic value of the resistance $R_{ac,k}$ can be determined either from joint experiments with multiple specimens or by FE analysis using either a stress-based or fracture mechanics approach. In both approaches analysis is based on characteristic values of results from material and fracture mechanics tests, and it must be validated in terms of compatible and permissible failure mode by joint experiments.

2.3. Principles of stress-based approach

The design values of out-of-plane (peeling) and in-plane shear stresses $\sigma_{z,t,Ed}$ and $\tau_{xy,Ed}$, respectively, should be obtained in stress analysis using FE models where appropriate mesh is used to obtain consistent stress values in zones of stress concentrations. Homogenized material properties may be and material orthotropy should be considered. A failure criterion to be applied in the failure plane of lap-shear connections exhibiting fibre-tear failure may be defined as:

$$\left(\frac{\sigma_{z,t,Ed}}{f_{z,t,d}}\right)^2 + \left(\frac{\tau_{xy,Ed}}{f_{xy,v,d}}\right)^2 \leq 1{,}0 \qquad (1)$$

The design values of out-of-plane and in-plane shear strengths $f_{z,t,d}$ and $f_{xy,v,d}$ should be determined in material tests with identical failure mode and plane as in joint experiments used for validation, considering statistical size effects governed by the type of stress distribution.

2.4. Principles of fracture-mechanics based approach

A design based on fracture mechanics uses a criterion where design values of the strain energy release rate for Mode I and Mode II obtained in FE models are compared to design values of critical strain energy release rates obtained from fracture mechanics tests, e.g. DCB and ENF tests:

$$\left(\frac{G_{I,Ed}}{G_{Ic,Rd}}\right)^m + \left(\frac{G_{II,Ed}}{G_{IIc,Rd}}\right)^n \leq 1.0 \qquad (2)$$

Virtual crack closure technique (VCCT) or cohesive zone modelling (CZM) can be used in FE models - the former for crack initiation and the latter for both crack initiation and propagation.

2.5. Limitations

The main limitation of the stress-based approach is the difficulty to account for size effects related to sharp stress peaks. Empirical solutions exist with factors to take those aspects into account for a limited number of overlap geometries, sizes, and material compositions.

VCCT analysis lacks the possibility to account for fibre bridging, requires the definition of a critical zone comprising a pre-crack, and in general is sensitive to pre-crack and mesh size. Analysis using CZM solves the problem of definition of the critical location and in general is less sensitive to mesh size. The main challenge is to define and validate parameters of the traction-separation law from fracture mechanics tests that properly defines the fibre bridging behaviour. The design example shown here compares results of the stress-based fracture mechanics (CZM) approach on a relatively simple joint.

3. Design example of verification of double-lap adhesive joint

The design resistance of a balanced double-lap adhesive joint with pultruded adherends when subjected to axial tension loading is determined by following the procedures described above with the use of Abaqus 2019 software. The geometry of the joint is taken from the experimental work performed in [1] and it is illustrated in Figure 1.

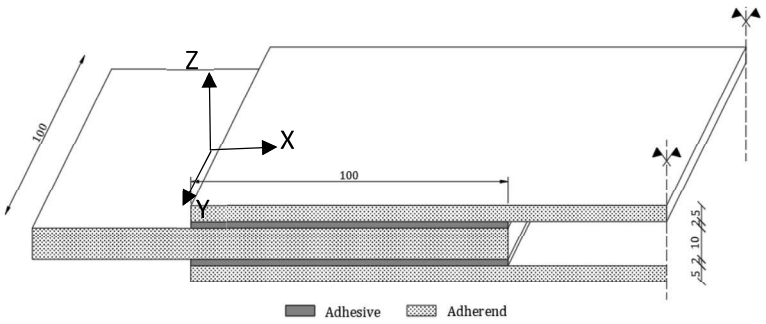

Figure 1. Geometry of half of the double-lap joint

For the given geometry, five experiments were conducted in [1] and fibre-tear failure occurred at 0,5 mm inside the inner adherend at approximately 158 kN load. The crack path was located within the first mat layer (Path I from [2]).

3.1 Joint description

Three symmetry boundary conditions are used, as indicated in Figure 2. Half of the width, half of the thickness, and half of the length of the physical joint are modelled, 1/8 of the complete joint, to reduce the computation time. The two interfaces between the adhesive and the inner and outer adherends are tie constrained.

The adherends are subdivided into six layers and two regions with different elements and sizes are chosen based on a mesh sensitivity analysis, see Figure 3. A relatively fine mesh with an element size of 0,25 mm is chosen at the bonded area, to capture the stress peaks at the end of the bond lines. Eight elements through the thickness of the 2 mm adhesive layer are modelled.

The three-dimensional 8-node linear brick element with reduced integration, C3D8R, is used for all the parts in the region of the fine mesh. The coarse region is meshed with 2 mm 4-node linear tetrahedron elements, C3D4.

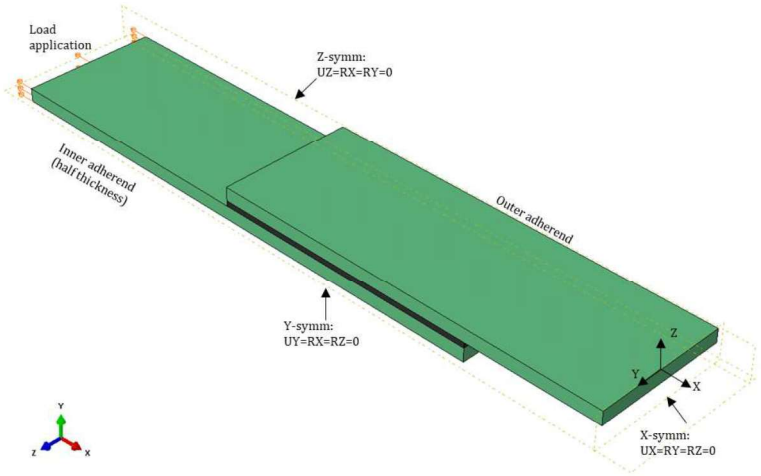

Figure 2. 1/8 model of the double-lap joint

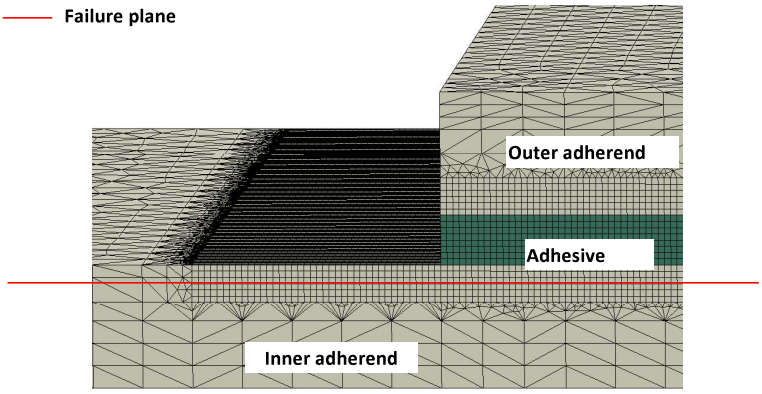

Figure 3. Detail of FE mesh of joint model

3.2 Stress-based approach

3.2.1 Design values of material strength

Average values of 8,0 MPa and 19,3 MPa for the out-of-plane and the shear strength, respectively, at the failure plane embedded 0,5 mm inside the inner laminate were obtained from [2] with 7,92% of coefficient of variation. Therefore, by applying the formula C.15 from prEN 1990 and considering that 10 samples were tested, the characteristic value of the out-of-plane tensile and shear strength is equal to 6,85 MPa and 16,53 MPa, respectively.

The design value of the out-of-plane tensile and shear strength for fibre-tear failure 0,5 mm inside the inner adherend is calculated based on Subclause 12.4.5.3 Paragr. (3). Assuming that the partial factor for the resistance model is $\gamma_{M,ac} = 1{,}7$ and the total conversion factor, η_c, is equal to 1, the design values of material strength in the failure planed embedded 0,5 mm inside the 10 mm thick inner adherend are:

$$f_{\mathrm{z,t,d}} = \frac{\eta_c}{\gamma_{M,ac}} \cdot f_{\mathrm{z,t,k}} = \frac{1}{1{,}7} \cdot 6{,}85 = 4{,}03 \text{ MPa} \quad (3)$$

$$f_{\mathrm{xy,v,d}} = \frac{\eta_c}{\gamma_{M,ac}} \cdot f_{\mathrm{xy,v,k}} = \frac{1}{1{,}7} \cdot 16{,}53 = 9{,}72 \text{ MPa} \quad (4)$$

3.2.2 Homogenized material properties

A summary of the input data for the adherends and adhesive are shown in Table 1, provided as mean values from manufacturer's datasheets, Fiberline and SikaDur, respectively.

Table 1: Homogenized material data for adherends and adhesive.

Pultruded adherends	$E_{x,t,m}$ = 24,0 GPa	$E_{y,t,m}$ = 7,0 GPa	$G_{xy,m}$ = 3,0 GPa	$v_{xy,m}$ = 0,07
Adhesive	E_m = 4,6 GPa		G_m = 1,7 GPa	v_m = 0,37

The stresses in the elements at the failure plane located 0,5 mm inside the inner adherend are read to obtain the design values of the applied action. For example, the S33 stresses, which correspond to the out-of-plane stresses in the adherend, are shown in Figure 4.

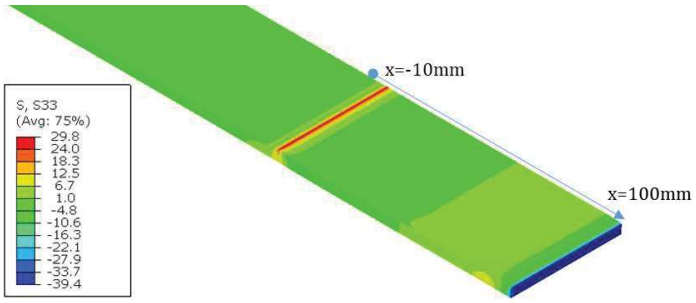

Figure 4. Out-of-plane stresses [MPa] at 0,5 mm inside inner adherend; at 100 kN load level

Due to fairly constant stress distribution along the width of the joint, a line along the middle of the joint (in the symmetry plane, see indication in Figure 4) is used to represent the stress values as a function of the bond length in Figure 5 by solid lines for the homogeneous material data.

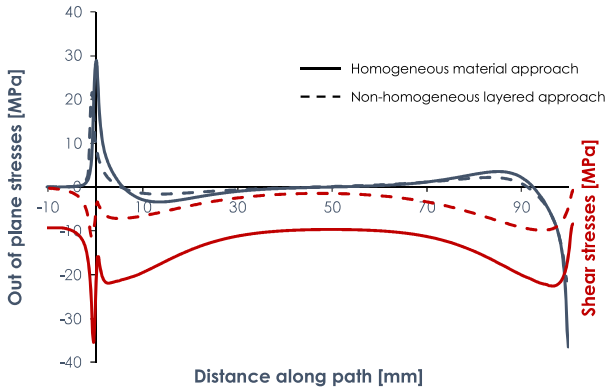

Figure 5. Stresses along bondline 0,5 mm inside inner adherend; at 100 kN load level

The design resistance of the joint for ULS verification is calculated by adjusting the load such that the stress-based quadratic criterion is equal to 1,0. In this specific case, an epoxy adhesive is used for a double-lap joint of 100 mm overlap length which results in sharp stress peaks at the bondline ends. Therefore, according to [2, 3], the two correction factors k_σ = 4,0 and k_τ = 2,0 are selected to take into account the size effect on strength. The maximum ratio of action vs. resistance is found at the location x=0 mm due to the shift in the peak values of the out-of-plane and shear stresses corresponding to the location where the adhesive layer begins. The ratio of action vs. resistance for the critical location is:

$$\left(\frac{\sigma_{z,t,Ed}}{k_\sigma \cdot f_{z,t,d}}\right)^2 + \left(\frac{\tau_{xy,Ed}}{k_\tau \cdot f_{xy,v,d}}\right)^2 = \left(\frac{27,5}{4 \cdot 4,03}\right)^2 + \left(\frac{17,5}{2 \cdot 9,72}\right)^2 = 2,91 + 0,81 = 3,72 \quad (5)$$

The ULS criterion is not satisfied with the load equal to 100 kN because the criterion given in Eq. (3) is exceeded at the critical location. The values of stresses obtained in the used FE model are linearly dependent on the applied load. Therefore, the design value of resistance for this failure mode can be determined by adjusting the applied load. Since the quadratic mixed-mode criterion is used, the applied load is to be divided by the square root of the obtained ratio of the action vs. resistance. Thus, the design resistance of this joint is equal to:

$$F_{Rd} = \frac{100}{\sqrt{3,72}} = 51,8 \text{ kN} \quad (6)$$

3.2.2.1 Non-homogeneous layered model

The layer-wise material properties of pultruded adherends are tabulated below. The thickness of each layer is listed in Table 2, provided as mean values from literature [4].

Table 1. Input material data for pultruded adherends.

Layer	$E_{x,t}$	$E_{y,t}$	$E_{z,t}$	G_{xy}	G_{yz}	ν_{xy}	ν_{yz}
1st combi-mat (0,5 mm)	12,8 GPa	12,8 GPa	3,2 GPa	6,2 GPa	1,4 GPa	0,27	0,36
2nd combi-mat (1 mm)	15,1 GPa	15,1 GPa	3,2 GPa	6,7 GPa	1,4 GPa	0,27	0,36
UD Roving (remaining)	38,9 GPa	3,2 GPa	3,2 GPa	2,7 GPa	1,4 GPa	0,32	0,27

Figure 5 also shows the calculated out-of-plane (peel) and in-plane shear stress distributions at the load of 100 kN with dashed lines. The values are taken from the same longitudinal path as indicated in Figure 4 i.e., in the middle of the width of the double-lap joint.

Applying the same design values of the out-of-plane tensile and shear strength, the maximum ratio of action vs. resistance at 100 kN load level at the critical location of the bondline end inside the inner adherend is calculated as shown in Eq. (7). Thus, the design resistance of the joint using layer-wise modelling and stress-based approach is given in Eqs. (7) and (8).

$$\left(\frac{\sigma_{z,t,Ed}}{k_\sigma \cdot f_{z,t,d}}\right)^2 + \left(\frac{\tau_{xy,Ed}}{k_\tau \cdot f_{xy,v,d}}\right)^2 = \left(\frac{21,9}{4 \cdot 4,03}\right)^2 + \left(\frac{7,7}{2 \cdot 9,72}\right)^2 = 2,00 \quad (7)$$

$$F_{Rd} = \frac{100}{\sqrt{2,0}} = 70,7 \text{ kN} \quad (8)$$

3.3 Fracture-mechanics approach

The 3D FE model described above is adapted such that it will allow for non-linear progressive failure analysis. In that respect, the quasi-static analysis using explicit dynamic solver with mass-scaling in Abaqus/Explicit is used to assure feasible convergence. CZM interface is applied at the failure plane e.g., 0,5 mm inside the inner adherend. The same material properties as defined in Section 3.2.2.1 are applied for the pultruded profiles and the adhesive layer.

To define the behavior of the CZM, a traction-separation law with design values of critical strain energy release rates at initiation and propagation were introduced as shown in Figure 6. A

  doi:10.5075/epfl-298799_978-2-9701614-0-0

trilinear traction-separation law is used for the CZM to account for the fibre-bridging behavior due to fiber-tear failure. Further subsections show how the CZM parameters are derived.

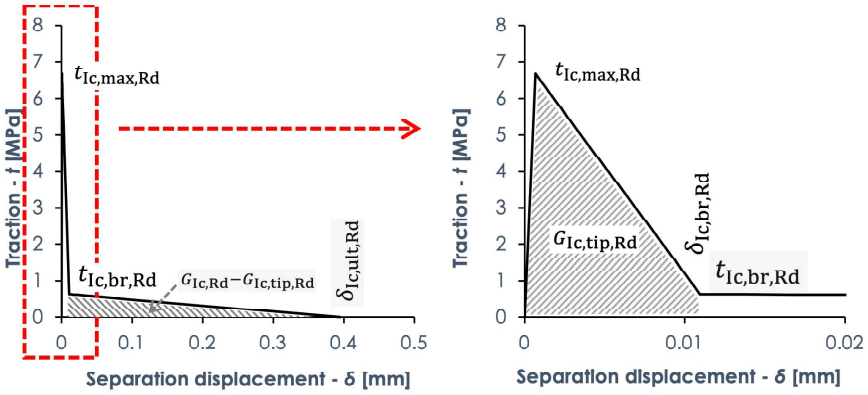

Figure 6. Traction-separation law for CZM with design values of critical parameters

3.3.1 Design values of critical strain energy release rate

Average values of 151 ± 35 J/m^2 and 536 ± 131 J/m^2 of Mode I critical strain energy release rate for crack initiation and propagation, respectively, were obtained from [4]. Therefore, by applying Eq. (C.15) from prEN 1990 and considering the number of tests, the characteristic values of the critical strain energy release rates for initiation and propagation correspond to 67,8 J/m^2 and 276,7 J/m^2.

The design value of the critical strain energy release rates for initiation and propagation of the fiber-tear failure inside the inner adherend is calculated based on Subclause 12.4.5.4 Paragr. (1). Considering the same partial and conversion factor as before, the values obtained are equal to 40 J/m^2 for initiation and 163 J/m^2 for propagation.

3.3.2 Design values of tractions and separations in CZM

The average value for the maximum traction is set equal to 25,2 MPa from [5] whilst 5-10% of that is considered as the fibre-bridging traction thus, 2 MPa. The design values of the tractions based on the proportion between average and design values of critical strain energy release rate are:

$$t_{\mathrm{Ic,max,Rd}} = \frac{G_{\mathrm{Ic,tip,Rd}}}{G_{\mathrm{Ic,tip,m}}} \cdot t_{\mathrm{Ic,max,m}} = \frac{40}{151} \cdot 25{,}2 = 6{,}7 \text{ MPa} \quad (9)$$

$$t_{\mathrm{Ic,br,Rd}} = \frac{G_{\mathrm{Ic,Rd}} - G_{\mathrm{Ic,tip,Rd}}}{G_{\mathrm{Ic,m}} - G_{\mathrm{Ic,tip,m}}} \cdot t_{\mathrm{Ic,max,m}} = \frac{163-40}{536-151} \cdot 2 = 0{,}64 \text{ MPa} \quad (10)$$

This results in the corresponding separations at damage initiation and bridging of the fibre-tear failure inside the inner adherend:

$$\delta_{\mathrm{Ic,br,Rd}} = \frac{2 \cdot G_{\mathrm{Ic,tip,Rd}}}{t_{\mathrm{Ic,max,Rd}}} = \frac{2 \cdot 40/1000}{6{,}7} = 0{,}012 \text{ mm} \quad (11)$$

$$\delta_{\mathrm{Ic,ult,Rd}} = \frac{2 \cdot (G_{\mathrm{Ic,Rd}} - G_{\mathrm{Ic,tip,Rd}})}{t_{\mathrm{Ic,br,Rd}}} = \frac{2 \cdot (163-40)/1000}{0{,}64} = 0{,}384 \text{ mm} \quad (12)$$

3.3.3 Design resistance of the joint and design force at crack initiation

The model ran until failure and therefore the design resistance of the joint is obtained by observing the damage of the interface and the obtained load displacement behavior. The force-

displacement graph resulting from FE analysis of the joint is shown in Figure 7. A slight change of stiffness is noticed at a design load of 32,1 kN corresponding to crack initiation.

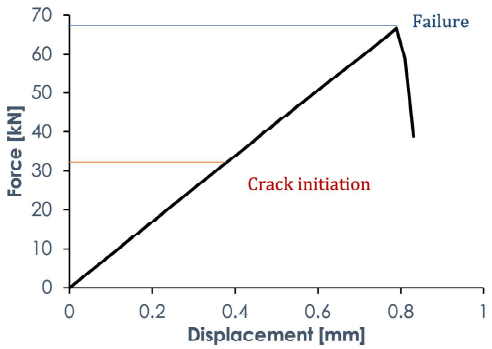

Figure 7. Numerically obtained force displacement graph with application of CZM

3.4 Validation of numerically determined design resistance with experimental data

Based on the available experimental results in [1], the design value of resistance of the given connection is calculated based on a partial factor of 1,7 and the variation of results and number of tests in the joint experiments. More specifically, five experiments were performed for this adhesively bonded joint geometry with a variation of results equal to V_x=13,5%. Thus, the characteristic value of resistance of the joints based on the tests is equal to 114,5 kN. Therefore, the design value of the resistance is given by:

$$F_{\mathrm{d}} = \frac{\eta_c}{\gamma_{M,ac}} \cdot F_k = \frac{1}{1{,}7} \cdot 114{,}5 = 67{,}3 \text{ kN} \quad (13)$$

4. Conclusions

The design value of resistance obtained in joint experiments is 67,3 kN which is 23% higher than the design resistance obtained by the stress-based approach using the design values of homogenized material properties and 5% lower than the corresponding one using the non-homogeneous properties in a layer-wise approach. The layer-wise modelling leads to a higher predicted resistance which however cannot be generalized. Lower stiffness of the material located next to the failure plane in the layer-wise approach leads to a reduction of the stress concentrations and thus increases the predicted joint resistance. The fracture mechanics approach using CZM predicts the design value of resistance corresponding to full crack propagation equal to 66,7 kN which is only 1% higher than the design value of resistance obtained in the joint experiments.

5. References

1. Keller T, Vallee T. Adhesively bonded lap joints from pultruded GFRP profiles. Part I: Stress-strain analysis and failure modes. Composites Part B. 2005, 36(4), 331-340.
2. Keller T, Vallee T. Adhesively bonded lap joints from pultruded GFRP profiles. Part II: joint strength prediction. Composites Part B. 2005, 36(4), 341-350.
3. Vallee T. Adhesively bonded lap joints of pultruded GFRP shapes. EPFL PhD thesis no. 2964, Lausanne, 2004.
4. Shahverdi M, Vassilopoulos AP, Keller T. Mixed-mode quasi-static failure criteria for adhesively-bonded pultruded GFRP joints. Composites Part A. 2014, 59, 45-56.
5. Cameselle-Morales A, et al. Numerical simulation of two-dimensional in-plane crack propagation in FRP laminates. Composite Structures. 2018, 200, 396-407.

